Detecting anomaly targets using handheld frequency domain electromagnetic system

Qu Xiaodong [a,b,*], Chen Wang [a,b], Fang Guangyou [a], Yin Hejun [a]

[a] Key Laboratory of Electromagnetic Radiation and Sensing Technology, Institute of Electronics, Chinese Academy of Sciences, Beijing 100190, China
[b] University of Chinese Academy of Sciences, Beijing 100049, China

ARTICLE INFO

ABSTRACT

In this paper, a handheld frequency domain electromagnetic system CEM-2 is presented for subsurface investigation (within less than 2 m). CEM-2 system employs one set of 3 coplanar coils. The transmitter uses sinusoidal pulse width modulation technology to generate low total harmonic distortion and arbitrary digital signal waveform. It is convenient to match different transmitting coils using the same circuit and system. The signal processing method can reduce some effects caused by unstable factors. Most operations are sum and product operation, contributing to high efficiency. The mounting positions of the metal items (a removable box, pre-amplifier) are selected according to the principle that primary magnetic field has minimum gradient. Experiments were conducted to evaluate the CEM-2 system. The response decreases as the operation frequency increases. The in-phase response changes with frequency faster than quadrature response. When the major axis of a target is in parallel with the system, the response is the strongest while the response is the weakest when the target is perpendicular to the system. This is because the effective conductivity is different due to de-polarization factor under primary field from different incident direction. Furthermore, results in a simulated test site indicate that CEM-2 can give distinct signatures for abnormal targets.

© 2017 Elsevier B.V. All rights reserved.

1. Introduction

During the world war, many unexploded ordnances have been buried in shallow ground that bring potential threats to human beings [1]. In modern society, subsurface detection for pipes, cables and public facilities underground has been drawing more and more attention. Thus, it is necessary to find a way to figure out the underground structure.

Main technologies for UXO detection are magnetic detection method [2–5], electromagnetic induction method (EMI) [6,7], and ground penetrating radar (GPR). Being in geomagnetic field, the UXO can be magnetized and generates static magnetic field. The perturbation caused by the UXO can be detected by fluxgate, optical pumping magnetometer, and so on. EMI method [8] measures the perturbation caused by abnormal targets being in the primary field generated by the transmitter and provides superior advantages for shallow subsurface investigation. EMI method operates both in time domain and frequency domain. UXO detection systems in time domain are mainly by Geonics. EM61 systems [9] generate primary magnetic field by air coil. The transmitting current is bipolar rectangle wave with duty ratio is about 25%. The receiving coil is also air coil and picks up the secondary field at four different time gates. Other editions are EM61-MK2 [10], EM61HH-MK2 [11], EM61-MK2A, and EM63 [12]. Similarly, there exit time domain systems that base on airborne platform [13].

Frequency domain systems mainly include GEM-2 [14], GEM-3 [15], GEM-5 [16] designed by Geophex, EM31-MK2 [17], EM34-3 [17], EM38 [18] designed by Geonics and NEMFIS [19] system made in Russia. EM31-MK2 system contains a transmitting coil and a receiving coil and works at 9.8 kHz and the offset distance is 3.66 m. EM34-3 system works at 6.4 kHz, 1.6 kHz and 0.4 kHz and the offset distances are 10 m, 20 m, 40 m respectively. EM38 system works at 14.5 kHz, including one transmitting coil and two receiving coils. Thus, EM systems image the subsurface structure at different depth by changing the offset between transmitter and receiver, which is called geometry sounding [20]. Thus, the operation and implements are usually complex. By contrast, GEM-2, GEM-3, and GEM-5 systems operate in frequency domain at 330 Hz ~ 96 kHz, including bucking coils which are used to balance out the primary field at the receiving coil. GEM Series systems can map underground struc-

Fig. 1. CEM-2, a handheld broadband frequency domain system.

ture with frequency sounding [20,21] method that measures the response at different operating frequencies utilizing a single set of coils. Therefore, this kind of systems can be made in a compact structure so that it is convenient for operation due to light weight and small size. At present, frequency domain electromagnetic systems have been widely used to detect unexploded ordnance [22,23] and buried drums containing hazardous waste [24], map shallow surface [25], and engage in archaeological studies.

In this paper, the authors present a handheld broadband frequency domain system CEM-2 (Fig. 1) designed for subsurface investigation. The CEM-2 employs a single set of three coplanar coils which means that CEM-2 is a compact, small volume and light weight instrument system. It is suitable for one person operation and efficient in field detection, especially in increasingly inaccessible areas. Furthermore, CEM-2 utilizes sine pulse-width modulation (SPWM) technology to generate arbitrary waveform (multi-frequencies combined waveform with arbitrary intervals) with low total harmonic distortion so that most of the power concentrates on the desired frequencies to improve the energy efficiency. Also, the SPWM technology does not depend on load, so it is convenient to match different transmitter coils using the same circuit and system. Alternatively, the bit-stream method [26] employed by GEM-2 needs more complicated algorithm and the algorithm depends on load. In addition, by convolution secondary field with standard sine and cosine time series and performing complex division between signal channel and reference channel, we can extract the in-phase and quadrature components of secondary field. The standard sine and cosine time series are pre-stored in the system, and we can call the time series directly to save processing time. The convolution between signals and standard time series rends a narrow-band matched filter. By doing complex division, the normalized in-phase response and quadrature response can be obtained. Thus, some unstable factors (such as the deformation of transmitter coil, the changes of transmitter current) that may induce false alarms can be cancelled out. All the data's analysis can be done in 1/25 s in a single DSP chip for real-time display and storage. Finally, the system is verified by experiments.

This paper is organized as follows. In section II, we describe the operation principle for frequency domain electromagnetic method briefly. Section III presents the main technologies and system designs in detail. Furthermore, simulation and experiment results are given in section IV and section V respectively followed by conclusions in section VI.

2. Operation principle

The system detects metal and magnetic anomaly targets by measuring the primary field's perturbation. The operation principle of frequency domain systems can be described by coupling between 3 coils [27], shown in Fig. 2. Here, TX is transmitter coil, RX is receiver coil, M_{TC}, M_{CR}, M_{TR} are mutual inductances between TX and target, target and RX, and TX and RX respectively, and K, K', K'' are transform coefficients of current to magnetic field.

If the equivalent inductance and resistance of the target coil are L_s, r_s, the in-phase component and quadrature component of the
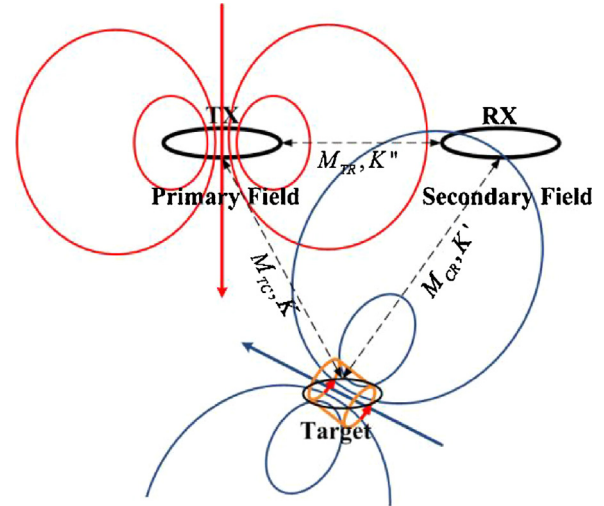

Fig. 2. Operation principle sketch map with 3 coils coupling.

secondary field H_s elative to primary field H_p can be written as follows:

$$Re\left(\frac{H_s}{H_p}\right) = -\frac{K'M_{TC}}{K''}\frac{\omega^2 L_s}{r_s^2 + \omega^2 L_s^2} \tag{1}$$

$$Im\left(\frac{H_s}{H_p}\right) = -\frac{K'M_{TC}}{K''}\frac{\omega r_s}{r_s^2 + \omega^2 L_s^2} \tag{2}$$

3. System design

Fig. 3 shows the electronic block diagram and the internal sensors layout of CEM-2. The system contains a transmitter system, a receiver system and magnetic field sensors.

Fig. 4 shows the diagram of transmitter system, which mainly includes DSP control unit, driver circuit, H-bridge circuit and transmitter coil.

CEM-2 can generate arbitrary single or multi-frequencies current waveforms. The transmitter employs sinusoidal pulse width modulation (SPWM) technology [28] to produce the desired current waveform with low total harmonic distortion (THD). The software in DSP converts the desired frequencies to switching signals (square pulses with adjustable duty cycle) according to the irregular sampling principle. The switching signals control H-bridge circuit that consists of four CMOSs connected across the transmitting coil to generate a synthetic complex waveform. To meet the requirement for magnetic moment, the transmitter coil consists of four 100-turn coils in parallel with inductor L = 3 mH, resistance R = 1.765 Ω. Finally, an example for five frequencies (from 275 Hz to 2075 Hz) synthetic transmitter current waveform is shown in Fig. 5(a), whose power spectrum density (PSD) is in Fig. 5(b). We can find that the maximum current is close to 1.3 A and the signal to noise ratio is about 85 dB.

Fig. 6 shows the scheme diagram of receiver system and magnetic field sensors, mainly including DSP/FPGA control module, data acquisition module (ADC), data transmission module (Bluetooth),
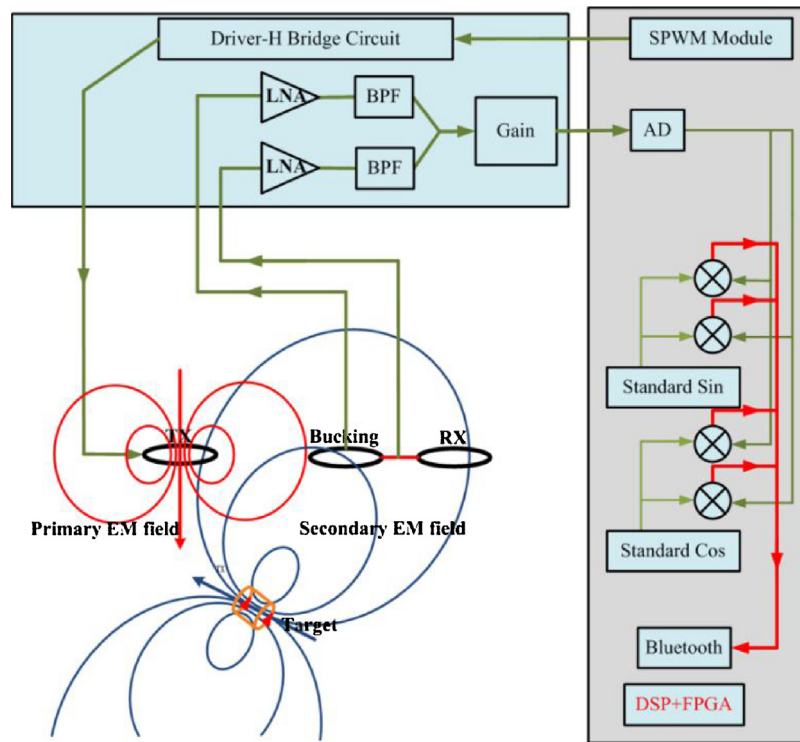
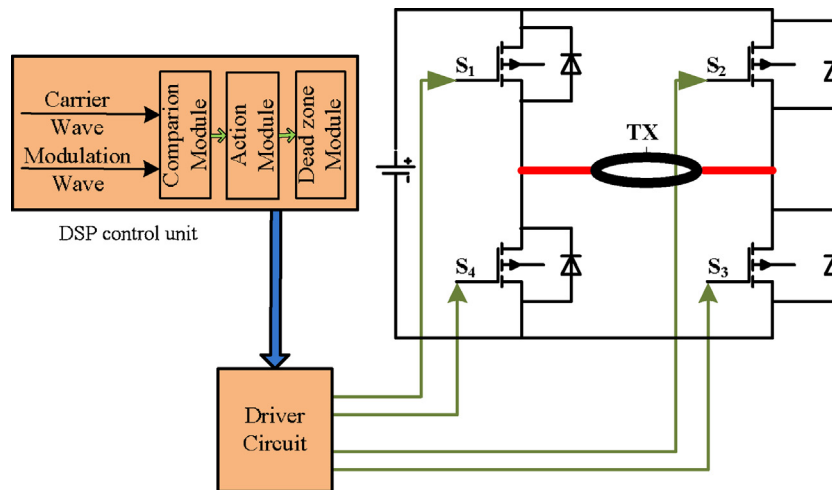**Fig. 3.** CEM-2 electronic block diagram and internal sensors layout.

Fig. 4. The scheme diagram of transmitter system.

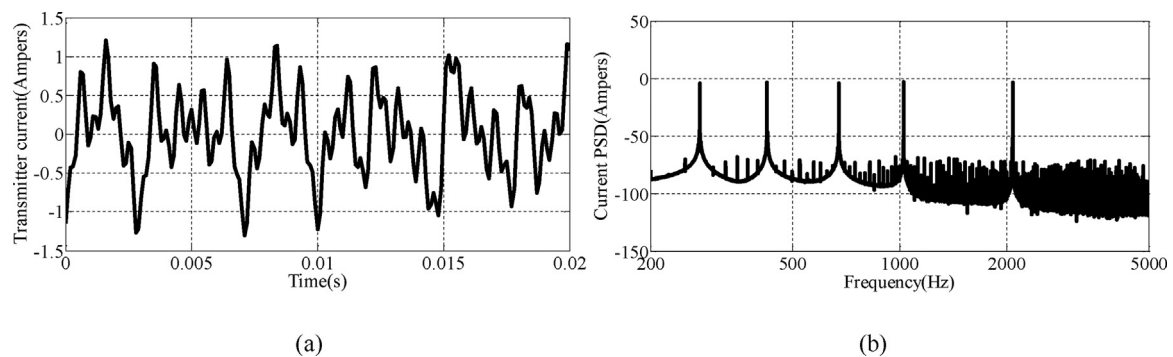(a)   (b)

Fig. 5. Test results for transmitter system: (a) An example for five frequencies synthetic current waveform; (b) Power spectrum density of the current waveform.
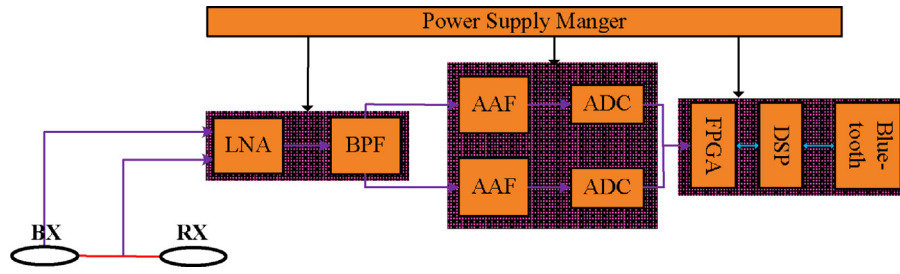
Fig. 6. The scheme diagram of receiver system.

anti-aliasing filter (AAF), signal conditioning module and induction magnetic field sensors (Bx and Rx).

CEM-2 has two channels that are both digitized at a sample rate of 78.125 kHz with 24-bit resolution: one is called the signal channel from the differential connection between the bucking coil and the receiver coil (secondary field) and the other is called the reference channel from the bucking coil (primary field). A FPGA chip coordinates controls for receiver circuits while a DSP chip coordinates controls for transmitter circuits and Bluetooth circuit and computes to extract in-phase and quadrature components. FPGA is a slaver of DSP and they exchange data via data bus and address bus. Then, complex computation is implemented in a single DSP chip for real time processing. Finally, the extracted in-phase and quadrature components are transferred to PDA by Bluetooth for display and storage.

The system employs one set of three coplanar coils which are designed to have a resonance frequency higher than the system bandwidth (200 Hz ∼ 20 kHz). The bucking coil which is about 1.06 m from transmitter coil plays two roles. Firstly, it is used as a bucking channel, wounding with less number of turns, and its output is mainly treated as primary field and balances out most of the primary field in signal channel. Secondly, it is used as a reference channel for locating near the transmitter coil. In this way, its output offers reference signal used in data processing. The signal channel is designed to produce zero output in free space and the relationship between the two coils is:

$$\frac{A_R N_R}{X_R^3} = \frac{A_B N_B}{X_B^3} \tag{3}$$

where A_i $(i = R, B)$ is the coil area, N_i $(i = R, B)$ is the number of turns, and X_i $(i = R, B)$ is the offset distance to the transmitter coil. It is not necessary to reduce all primary field and this method typically can balance out about 40 dB [29], achieving the same order of primary and secondary signals.

Signal conditioning module includes low noise amplifiers (LNA), analog band pass filters (BPF) and single-ended signal to differential signal converters. LNA is designed with differential amplifier INA163 and BPF is designed in Sallen-Key structure with operational amplifier opa2188. The noise performance of the integrated module is measured with a terminated input in a shielding barrel. The power density of the equivalent input noise is about $1.33 nv/\sqrt{Hz}$ shown in Fig. 7.

The support plate, made of wood that has small linear expansion coefficient [30], is about 180 cm*12 cm. As indicated, the ski also contains a signal conditioner circuit and a removable circuit box that contains control unit, data acquisition module and transmitter system. The mounting positions of the two boxes are selected according to the principle that primary magnetic field has minimum gradient. Assuming, the removable circuit box is r_1 to the transmitter coil and the distance between signal conditioner circuit and the transmitter coil is r_2, so we have:

$$(r_1, r_2) \in \min \nabla H_p \tag{4}$$

Thus, we select the position $r_1 = 0.62$ m and $r_2 = 1.3$ m. In this way, we can reduce false alarm rate caused by deformation of the support wood.

The system works at a sample rate of 78.125 kHz, producing a 3125 long time-series during 1/25 s. To obtain the in-phase and quadrature response from the two channels, we convolve the sampled time series with a preset of standard sine time series (in-phase component) and cosine time series (quadrature component) and then perform a complex division for each transmitting frequency.

The secondary field (S) generated by anomaly targets has same frequencies as primary field (P). The amplitude and phase of the secondary field mainly depend on transmitting magnetic moment, transmitter-receiver offset and targets' parameters. The signals picked-up by bucking coil and receiver coil are treated as a combination of S and P. If the transmitting frequency is $\omega = 2\pi f_0$, the signal in the receiver coil can be written as $a_1 \sin(\omega t + \varphi_1)$ and the signal in the bucking coil is $a_2 \sin(\omega t + \varphi_2)$. We extract the in-phase (I) and quadrature (Q) components in part per million (ppm) as:

$$I = 10^6 \left[\frac{a_1}{a_2} \cos(\varphi_1 - \varphi_2) - 1 \right]$$

$$Q = 10^6 \frac{a_1}{a_2} \sin(\varphi_1 - \varphi_2) \tag{5}$$

4. Simulation examples

The EM responses of vertical magnetic dipole excitation over a layered earth are given by ward and Hohmann [31]. Under quasi-static assumption, when the transmitter and receiver coils are at the same height h over a layered earth with magnetic moment M, the induced secondary magnetic field Hz at the receiver coil can be written as:

$$H_z = \frac{M}{4\pi} \int_0^\infty \left[1 + R(\lambda) e^{-2\lambda h} \right] \lambda^2 J_0(\lambda \rho) d\lambda \tag{6}$$

where ρ is the distance between transmitter coil and receiver coil, J_0 is the Bessel function of the first kind of order zero, and the kernel function $R(\lambda)$ can be obtained by recurrence relation. So, the secondary field H_s normalized against the primary field H_p can be written as follows:

$$\frac{H_s}{H_p} = \rho^3 \int_0^\infty R(\lambda) e^{-2\lambda h} \lambda^2 J_0(\lambda \rho) d\lambda \tag{7}$$

The EM responses of vertical magnetic dipole excitation over a solid sphere are given by Grant and West [32]. The picked-up secondary magnetic field H_{sz} by the receiver coil can be written as:

$$H_{sz} = \left(H_{r,r} + H_{\theta,r} \right) \cos \theta_r - \left(H_{r,\theta} + H_{\theta,\theta} \right) \sin \theta_r \tag{8}$$
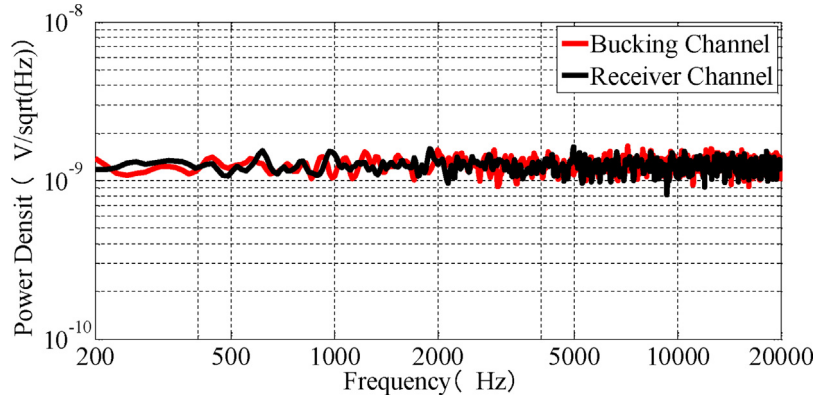
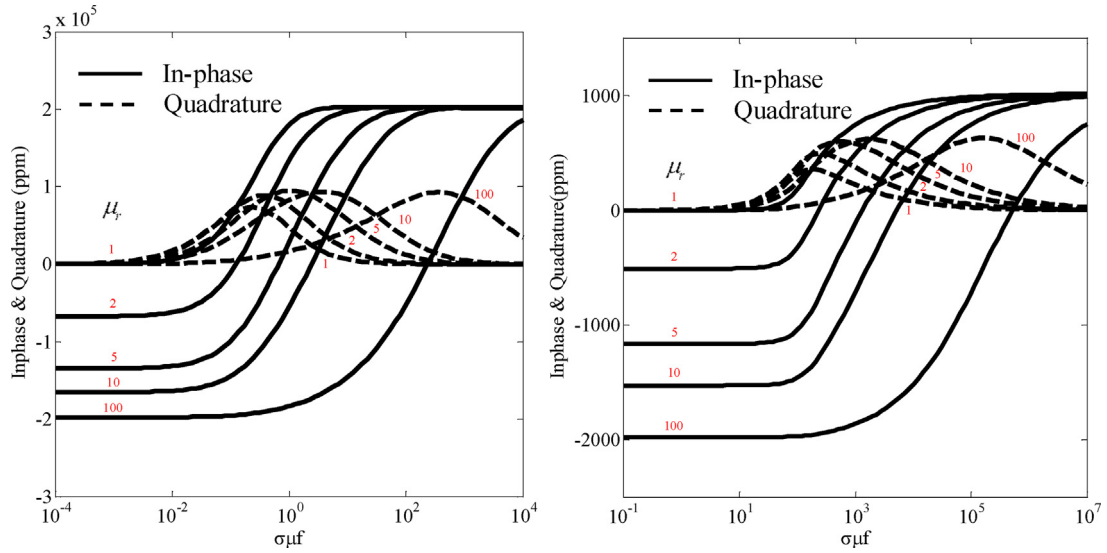Fig. 7. Power density of equivalent input noise.

Fig. 8. In-phase (solid curves) and quadrature (dashed curves) components of the secondary field: (a) over a homogeneous half-space; (b) over a solid sphere.

where $H_{i,j}$ $(i, j = r, \theta)$ represents j components of the secondary field from i dipole source. Grant and West give the expressions for calculation as follows:

$$H_{r,\theta} = -\frac{M_r}{4\pi} \sum_{n=1}^{\infty} (X_n + iY_n) \frac{a^{2n+1}}{(rr_0)^{n+2}} nP_n^1 (\cos\theta) \tag{9a}$$

$$H_{r,\theta} = \frac{M_r}{4\pi} \sum_{n=1}^{\infty} (X_n + iY_n) \frac{a^{2n+1}}{(rr_0)^{n+2}} nP_n^1 (\cos\theta) \tag{9b}$$

$$H_{r,\theta} = \frac{M_\theta}{4\pi} \sum_{n=1}^{\infty} (X_n + iY_n) \frac{a^{2n+1}}{(rr_0)^{n+2}} nP_n^1 (\cos\theta) \tag{9c}$$

$$H_{\theta,\theta} = -\frac{M_\theta}{4\pi} \sum_{n=1}^{\infty} (X_n + iY_n) \frac{a^{2n+1}}{(rr_0)^{n+2}}$$
$$\times \left[n^2 P_n (\cos\theta) - \frac{n}{n+1} \cot(\theta) P_n^1 (\cos\theta) \right] \tag{9d}$$

where P_n is the nth order Legendre polynomial and P_n^1 is the associated Legendre polynomial.

In addition, for a solid sphere with conductivity σ and permeability μ, we have the following expression:

$$X_n + iY_n = \frac{\left[\frac{1}{2} - \mu_r (n+1) \right] I_{n+1/2} (ka) + ka I'_{n+1/2} (ka)}{\left(\frac{1}{2} + n\mu_r \right) I_{n+1/2} (ka) + ka I'_{n+1/2} (ka)} \tag{10}$$

where $k^2 = i\omega\mu\sigma$ and $I_{n+1/2} (ka)$ is the modified spherical Bessel function of the first kind.

Then, the secondary field H_{sz} normalized against the primary field H_p and the result is:

$$\frac{H_{sz}}{H_p} = \frac{4\pi\rho^3}{M} H_{sz} \tag{11}$$

Fig. 8 shows I and Q as functions of $\sigma\mu f$ for the CEM-2 configuration with $\rho = 1.67$ m and $h = 1$ m over a homogeneous half-space (Fig. 8(a)) or over a solid sphere (Fig. 8(b)). We can find that the secondary field becomes dominated by magnetization effect as $\sigma\mu f \to 0$, so the in-phase response becomes frequency independent; meanwhile, the quadrature component goes to zero because of the disappearance of eddy currents. By contrast, the secondary field becomes dominated by conductive effect as $\sigma\mu f \to \infty$, so the in-phase response becomes converge; and, the quadrature component goes to zero due to small skin depth. However, under middle $\sigma\mu f$, both the magnetization and conductive effects have impact on the secondary field with frequency dependent in-phase and quadrature response.
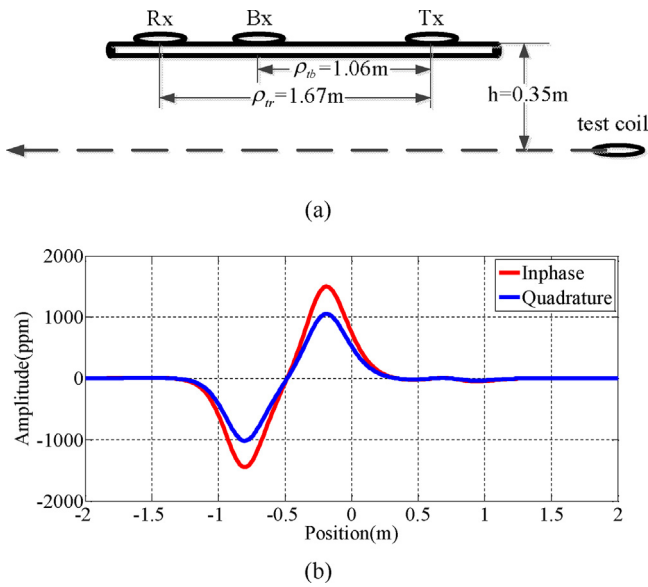
Fig. 9. Simulation with a standard coil with known parameters: (a) simulation scenario; (b) Simulation I and Q results.
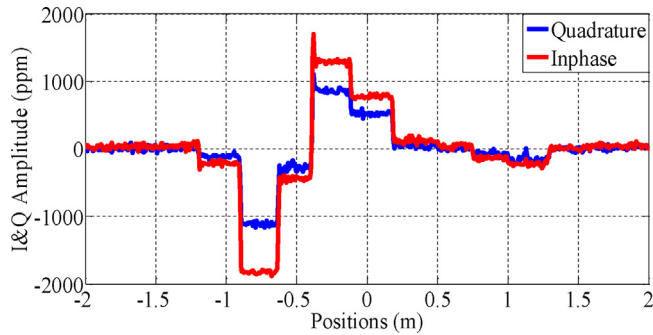
Fig. 10. The experiment results for CEM-2 with standard test coil.

To depict the signature of in-phase and quadrature components during detection, we illustrate another simulation example for the CEM-2 configuration with a standard coil. The test coil's parameters are: r = 455.4 Ω, L = 217.5 mH. Fig. 9(a) shows the simulation scenario, where Rx is receiver coil, Bx is bucking coil and Tx is transmitter coil. When transmitting magnetic moment is 3Am² and operation frequency is 475 Hz, the simulation results for in-phase and quadrature response are shown in Figure (9). The peak-to-peak response is 3500 ppm for in-phase and 2450 ppm for quadrature. The deviation between in-phase and quadrature component can also be verified by eq. 1 and eq. 2. Furthermore, when the test coil moves from the Tx side to Rx side, the I and Q components indicate that there is a minimum value under Tx, a positive peak under Bx and a negative peak under Rx.

5. Experiment results

To test the CEM-2 system performance, we have performed several experiments using the CEM-2 system.

5.1. Experiment with standard coil

We did the first experiment point-by-point using the same standard test coil as the simulation example Fig. 9. The test results are shown in Fig. 10. It is clear that the signatures of in-phase and quadrature response are consistent with the simulation results. On one hand, the peak-to-peak of in-phase response is 3150 ppm and
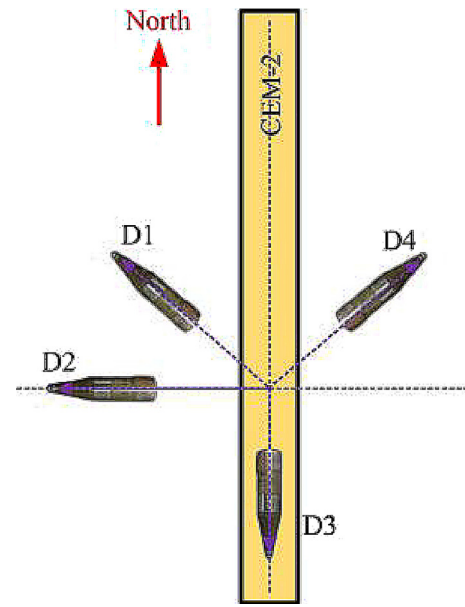
Fig. 11. Experiment scenario for CEM-2 under different target orientation.

quadrature response is 1970 ppm for CEM-2 in experiment which is a litter smaller than the simulation results. The most possible reason is that we do not take the distributed capacitance of the test coil into consideration during simulation. On the other hand, a local minimum point appears under Tx (at 1.06 m), a maximum point under Bx (at −0.13 m), and a minimum point under Rx (at −0.64 m). Furthermore, firstly, when the coil approaches the Rx, the amplitude becomes larger and larger (−2 m to −0.64 m); secondly, when the coil locates between Rx and Bx, the secondary signal increases from minimum to maximum across zero (−0.64 m to −0.13 m); thirdly, the response becomes from maximum to local minimum when moved from Bx to Tx (−0.13 m to 1.06 m); lastly, the response becomes weaker and weaker away from Tx (from about 1 m to right side).

5.2. The effect of operation frequency

We did an experiment under different operation frequencies from 275 Hz to 1075 Hz, in which the target is parallel with the system (D3 shown in Fig. 11). The CEM-2 system was kept horizontal at a height of 50 cm from the target. Fig. 12 shows the test results. It is clear that the peak-to-peak response of in-phase and quadrature components at all frequencies can find the target. Furthermore, the peak-to-peak responses decrease as the operation frequencies increase, but the in-phase responses reduce more slowly than the quadrature responses. Under low induction number, the response is proportional to $\sigma \mu f$ (shown in Fig. 8). However, the impedance of the load increases as the frequency because of inductive transmitter coil. As a result, the transmitter current decreases for a stable voltage across the load, which contributes to the reduction of response directly.

5.3. The effect of different orientation

We also did an experiment to study the effect of the different orientations of the target, as shown in Fig. 11. Similarly, CEM-2 was kept horizontal at a height of 50 cm from the target and the operation frequency is 475 Hz. The results are shown in Fig. 13, from where we can find that the response curves are in consistent with each other with different amplitudes under different directions relative to the system. This is because the induction number $\sigma \mu f$
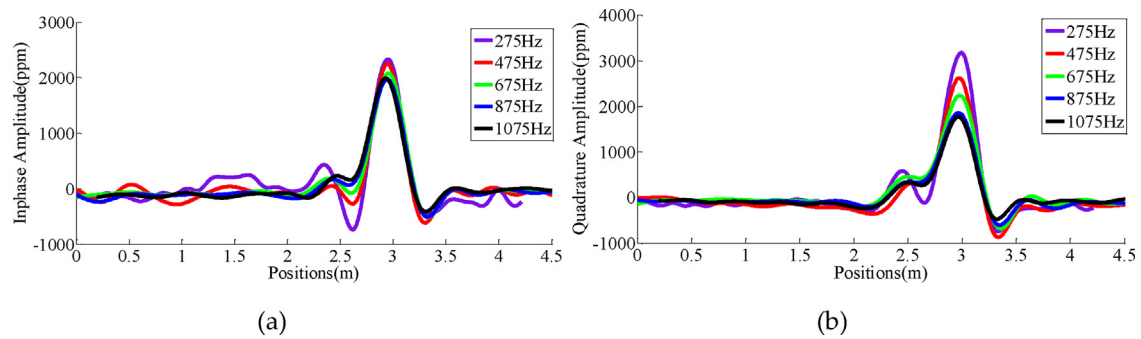
Fig. 12. Results for CEM-2 under different operation frequencies: (a) In-phase response; (b) Quadrature response.
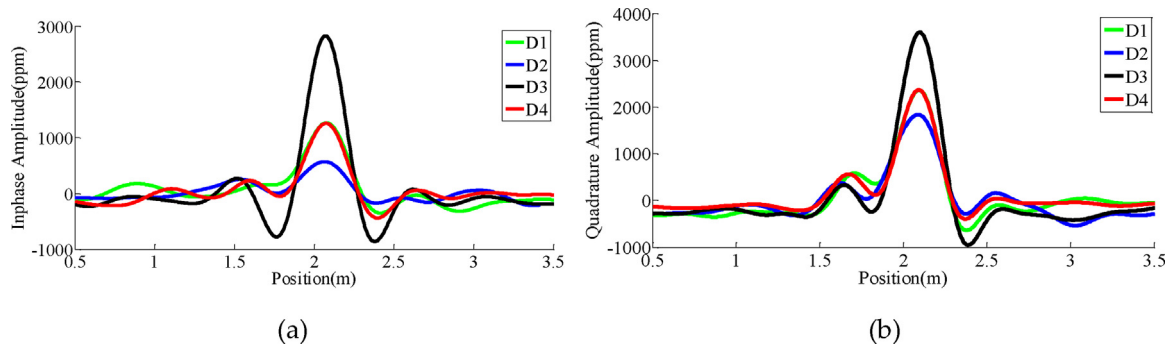

Fig. 13. Results for CEM-2 under different Orientations: (a) In-phase response;(b) Quadrature response.

changes as rotating from parallel to perpendicular to the system. For example, for a prolate ellipsoid, if the outer diameter is about 8 cm and length is about 30 cm in total (the same size as the target used in experiment), the depolarization and demagnetizing factors are L1 = 0.082 and L2 = L3 = 0.459. Thus, faced with primary field from different directions, the target's effective conductivity and permeability are different, resulting in different induction number. Further, by comparing the amplitudes of all kinds, we find that when the major-axis of the target is in parallel with the system, the response is the strongest. When the major-axis of the target is perpendicular to the system, the response is the weakest. The peak response of D1 and D4 are coincide with each other, indicating that when the target is the same angle biased left or right with respect to the system, the peak responses are the same. The in-phase response falls at a faster rate than quadrature response as induction number $\sigma\mu f$ decreasing which can also be verified in Figs. 8 and 12.

5.4. Experiment in simulated test site

The last experiment was implemented in a simulated test site, whose size is 5 m × 5.2 m. Six metal and magnetic targets with different size and materials are distributed in 5 survey lines like Fig. 14. The size of targets in the figure is not as big as the sketch map and the target T1 is placed in z direction. The descriptions of the targets are shown in Table 1. During the experiment, the system CEM-2 was kept horizontal at 80 cm height from the ground. The results is collected with 1 m line intervals and interpolated with Kriging method. The in-phase and quadrature results at 475 Hz are illustrated in Fig. 15.

As described above, when the CEM-2 system passes by the target along a survey line, a huge positive peak and negative local minimum point will appear. This signature can help us to distinguish the targets, for example, the red oval logos shown in Fig. 15.

The target L1 cannot be detected in-phase map while it is successfully detected in quadrature map. L1 is made up of aluminum whose relative permeability is about 1. The in-phase response is
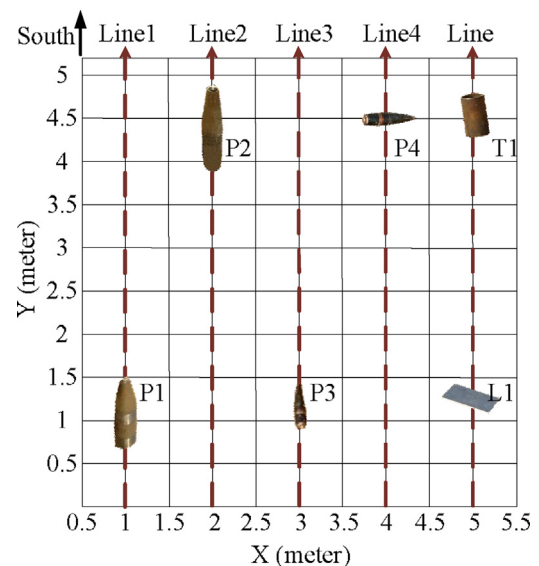

Fig. 14. The experiment test site.

mainly influenced by the relative permeability and the quadrature response is mainly proportion to the electrical conductivity. Thus, it is superior for quadrature component to detect the target L1. The target P4 is failed to be detected in both in-phase and quadrature map. On one hand, the outer diameter of P4 is about 1.2 cm and 6 cm in length. So, only weak eddy current can be induced in P4. On the other hand, P4's major axis is perpendicular to the CEM-2 system, reducing the response furthermore as shown in Fig. 13. As a result, the secondary field is difficult to be distinguished from the ambient noise.

However, there exist false positives (black oval) in several locations. Firstly, the main reason is that the eddy current induced by big targets can cover large footprint on near area. For example,
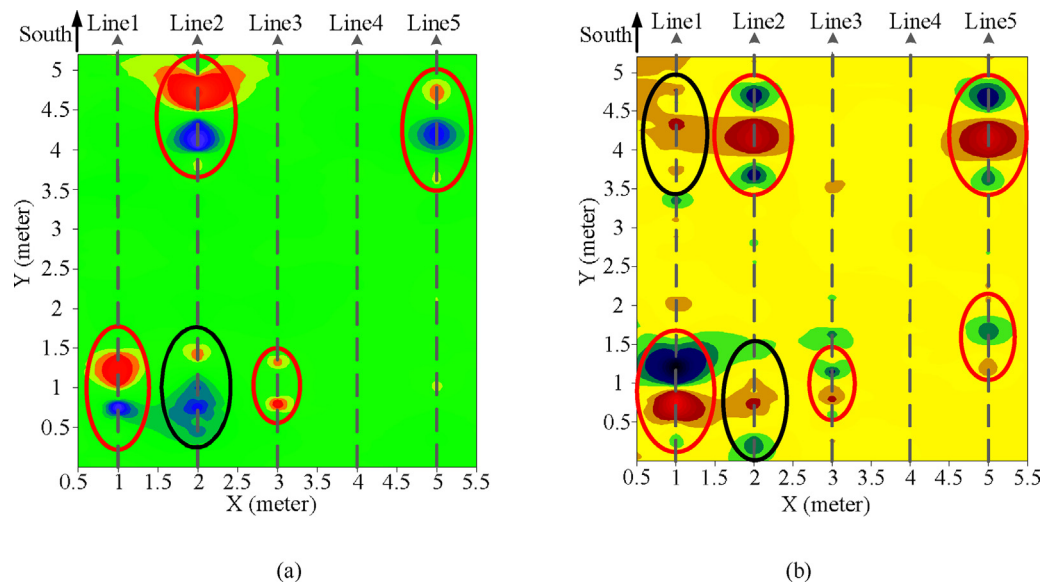
(a)   (b)

Fig. 15. The test results for a simulated test site with CEM-2: (a) In-phase response map; (b) Quadrature response map.

Table 1
Descriptions of targets used in the experiment.

Target ID	Description	X(m)	Y(m)
P1	OD [a] (8) × 35 cm steel horizontal, S-N [b]	1	1
P2	OD (10) × 56 cm steel 35°, S (up)-N	2	4.3
P3	OD (2) × 8 cm steel horizontal, S-N	3	1.2
P4	OD (1.2) × 6 cm steel horizontal, E-W	4	4.5
L1	22.3 × 14.5 cm aluminum sheet 12°, ES (up)-WN	5	1.2
T1	OD (10) × 20 cm ferromagnetic vertical	5	4.5

[a] OD means Outer Diameter.
[b] S-N means that the direction of head to nose is from south to north.

CEM-2 can detect P2 when surveying along Line1 and detect P1 along Line2. Secondly, the interpolation method may have impact on image quality. Thirdly, the height and motion noise can also contribute to the false anomaly. It is useful to take the following steps to avoid or reduce some false positives. On one hand, refine the area, and do detail detection to confirm one or more targets. On the other hand, keep CEM-2 horizontal at the same height as possible and reduce the instrument's motion noise during survey.

6. Conclusion

In this paper, we present a handheld broadband frequency domain electromagnetic system CEM-2 for subsurface investigation. The technologies employed are described in great detail. Especially, the system utilizes SPWM technology to generate the desired synthetic current signal. All the metal items are put on the support ski where primary magnetic field has minimum gradient. Most operations in processing method are sum and product operation, contributing to high efficiency. By using a standard test coil, the simulation results are consistent with the experiment results both in amplitude and trend. The response is affected by the operation frequency and the target's orientation. When the operation frequency increases, the response decreases because of the reduction of transmitting current. The response is strongest if the major axis of the target locates along with the system, and vice versa.

Experiments conducted in simulated test site indicate that CEM-2 can give distinct signatures and horizontal locations for abnormal targets. Thus, CEM-2 may provide great benefits in UXO detection, especially in increasingly inaccessible areas.

Conflict of interests

The authors declare that there is no conflict of interests regarding the publication of this paper.

Acknowledgment

References

[1] C. Chirgwin, Managing land mine and UXO contamination in exploration projects, Leading Edge 24 (2005) 376–377.
[2] F. Roy, Wiegert Man-Portable Magnetic Scalar Triangulation and Ranging System for Detection Localization and Discrimination of UXO[J], 2009.
[3] D.K. Butler, Implication of magnetic backgrounds for unexploded ordnance Detection[J], J. Appl. Geophys. 54 (2003) 111–125.
[4] W.E. Doll, J.R. Sheehan, T.J. Gamey, et al., Results of an airborne vertical magnetic gradient demonstration, new Mexico[J], J. Environ. Eng. Geophy. 13 (3) (2008) 277–290.
[5] W. Doll, Demonstration of an Enhanced Vertical Magnetic Gradient System for UXO[J], Demonstration of An Enhanced Vertical Magnetic Gradient System for Uxo, 2008.
[6] T. Bell, B. Barrow, J. Miller, et al., Time and frequency domain electromagnetic induction signatures of unexploded Ordnance[J], Sens. Imaging 2 (3) (2001) 153–175.
[7] L.R. Pasion, D.W. Oldenburg, Locating and Characterizing Unexploded Ordnance Using Time Domain Electromagnetic Induction[J], 2001.
[8] M.S. Zhdanov, Electromagnetic methods in the frequency and time domains, Methods Geochem. Geophys. 43 (2009) 649–693.
[9] A.B. Schwartz, C.M. Kennedy, Comparison of EM61 anomaly response signatures from different TX/RX coil Configurations[J], Phys. Ther. 80 (1) (2004) 1629–1640.
[10] H.H. Nelson, T. Bell, J. Kingdon, et al., EM61-MK2 Response of Standard Munition Items[J], 2008.
[11] T. Bell, B. Barrow, Proceedings. IGARSS 2000. IEEE 2000 International. IEEE Xplore, 2000:1433-1435, Subsurface Discrimination Using Handheld Electromagnetic Induction Sensors[C]//Geoscience and Remote Sensing Symposium, 2000, vol. 4, 2000.
[12] J.D. McNeill, Application of TEDM Techniques to Metal Detection and Discrimination: A Case History with the New Geonics EM-63 Fully Time-Domain Metal Detector. Geonics Ltd, Technical Note TN-32, 2000.

[13] L.P. Beard, W.E. Doll, T.J. Gamey, et al., Comparison Of Airborne Magnetic And Electromagnetic Systems For Ordnance Detection And Mapping[C]//Symposium on the Application of Geophysics to Engineering and Environmental Problems, Environment and Engineering Geophysical Society, 2008, pp. 1427.

[14] I.J. Won, D.A. Keiswetter, G.R.A. Fields, GEM-2: A new multi-frequency electromagnetic sensor, J. Environ. Eng. Geophys. 1 (1996) 129–137.

[15] I.J. Won, D.A. Keiswetter, D.R. Hanson, GEM-3: a monostatic broadband electromagnetic induction sensor, J. Environ. Eng. Geophys. 2 (1997) 53–64.

[16] H. Huang, B. Sanfilipo, I.J. Won, Planetary exploration using a small electromagnetic sensor, IEEE Trans. Geosci. Remote Sens. 43 (2005) 1499–1506.

[17] J.D. McNeill, Electromagnetic Terrain Conductivity Measurement at Low Induction Number, Geonics Ltd, Mississauga, Ontario, Canada, 1980, TN-6.

[18] J.D. McNeill, Archaeological Mapping Using the Geonics EM38 B to Map Terrain Magnetic Susceptibility, Geonics Ltd, Mississauga, Ontario, Canada, 2013 (TN-35).

[19] Y. Manstein, A. Manstein, EMI sensor NEMFIS: method, equipment and case stories of archaeological prospection, Archéosciences 33 (2009) 321–324.

[20] A.A. Kaufman, G.V. Keller, Frequency and Transient Sounding, Elsevier Science Publishes B.V, 1983.

[21] I.J. Won, Small frequency-domain electromagnetic induction sensors, Leading Edge 22 (2012) 320–322.

[22] D.K. Butler, Potential fields methods for location of unexploded ordnance, Leading Edge 20 (2001) 890–895.

[23] I.J. Won, V. Murphy, P. Hubbard, Geophysics and weapons inspection, Leading Edge 23 (2004) 658–662.

[24] R.L. Siegrist, D.L. Hargett, Application of surface geophysics for location of buried hazardous wastes, Waste Manage. Res. 7 (1989) 325–335.

[25] S.P. Sharma, K. Anbarasu, S. Gupta, Integrated very low-frequency EM, electrical resistivity, and geological studies on the Lanta Khola landslide North Sikkim India, Landslides 7 (2010) 43–53.

[26] N.D. Patel, U.K.A. Madawala, bit-stream based PWM technique for variable frequency sinewave generation, IEEE Trans. Ind. Electron. 56 (2009) 2530–2539.

[27] F.S. Grant, F.G. West, Interpretation Theory in Applied Geophysics, McGraw-Hill Book Co. Inc., 1965, pp. 486–492.

[28] M. Renge, H. Suryawanshi, M. Chaudhari, Digitally implemented novel technique to approach natural sampling SPWM, EPE J. 20 (2010) 13–20.

[29] I.J. Won, A. Oren, F. Funak, GEM-2A: A programmable broadband helicopter-towed electromagnetic sensor, Geophysics 68 (2003) 1888–1895.

[30] B. Thomas, D. George, An Electromagnetic Induction System for Observation of Bulk Magnetization Response of Uxo Targets, G&G Sciences Inc., 2012, MR-1711-IR.

[31] M.N. Nabighian, Electromagnetic methods in applied geophysics, Soc. Explor. Geophys. (1988) 130–311.

[32] F.S. Grant, F.G. West, Interpretation Theory in Applied Geophysics, McGraw-Hill Book Co Inc., 1965, pp. 515–520.

Biography

Xiaodong Qu received the B.S. degree from Xidian University, Xi'an, China, in 2012. He is currently pursuing the Ph.D. degree at the Institute of Electronics, Chinese Academy of Sciences, Beijing, China. His research interests include new technologies for electrical and magnetic geophysical prospecting and electromagnetic wave propagation in earth-ionosphere and seawater.